Formalism of the Kronig-Penney model for superlattices of variable basis

Perng-fei Yuh and K. L. Wang
Device Research Laboratory, Department of Electrical Engineering, University of California, Los Angeles, California 90024-1600

(Received 22 February 1988; revised manuscript received 7 July 1988)

A formalism of the Kronig-Penney model based on the transfer-matrix technique and the envelope-function approximation has been developed for superlattices. It can be used in handling superlattices composed of complicated bases, is easier to use than the conventional Kronig-Penney model in matching boundary conditions, and is more accurate because the effective mass and band coupling are included. The minibands of superlattices having different superlattice bases are analyzed by this new method.

I. INTRODUCTION

Superlattices are alternating ultrathin epitaxial layers, in which a one-dimensional potential is superimposed on the crystal potential of the background crystal.[1] The one-dimensional potential is formed by the band offset of the heterolayers in a compositional superlattice, or by periodically growing the *n*- and *p*-doped semiconductor layers, separated by intrinsic layers in the doped superlattice or *n-i-p-i*. While the real crystal potential has the same period as the lattice points, the period of the superlattice potential is the same as the alternating layers. For convenience, one period of the alternating layers will be called the basis of the superlattice. In the bulk semiconductor, different bases or primitive cells will result in different crystal potentials, thus different energy bands. Analogously, one may expect that the minibands in the superlattice will change as the superlattice basis changes. In the past since its inception in 1969,[2] the superlattice basis has always been simple barrier-well structure for simplicity of analysis. With modification of the basis, interesting effects are expected in the miniband transport and optical transitions.

The Kronig-Penney model has been applied to calculate the minibands in a superlattice with some modifications of the boundary conditions.[3,4] Those boundary conditions are derived from the envelope function approximations.[5] The wave equations and boundary conditions of three commonly used models are listed in Table I for later discussion. Among them, the effective-mass model takes into account the effective-mass difference in the barrier and the well regions. The two-band model includes the coupling of the conduction band and light-hole band. While the three-band model includes further the coupling of the split-off band. Since in the $\mathbf{k}\cdot\mathbf{p}$ theory the heavy-hole band is decoupled with the other three bands,[6] the three-band model is the most accurate of the three in treating all the four-band interactions. The modifications give simple final forms and need no more computation effort than the conventional Kronig-Penney model does.[7] However, both the classical Kronig-Penney model and the modified ones have the fundamental limitations. First, the formalism of the Kronig-Penney model is tedious and needs to simplify the determinant of a 4×4 matrix.[8] Secondly, it can only be used for a single square-well basis, but cannot be used for complicated bases, for example, bases with multiple layers, band-bending, or an arbitrary shape of the well by adjusting the alloy composition. With an increasing interest in applications of the novel superlattice or quantum well structures,[9-12] an accurate but simple model is necessary for theoretical predictions and explanation of experimental results.

A new formalism of the Kronig-Penney model, which uses the transfer matrix technique within the envelope-function framework is developed for general bases, and it

TABLE I. Wave equations and the boundary conditions for each of the envelope-function approximations. Those functions under the column of boundary conditions are continuous throughout the superlattice layers, and are used for Γ_1 and Γ_2 in Eq. (1).

Model	Wave equation	Boundary conditions Γ_1,Γ_2
Effective mass	$(E-V_s)\psi(z)+\frac{\hbar^2}{2}\left[\frac{\psi(z)'}{m^*}\right]'=0$	$\psi(z),\ \frac{\psi(z)'}{m^*}$
Two band	$(E-V_s)\psi(z)+\frac{2}{3}P^2\left[\frac{1}{E-V_p}\psi(z)'\right]'=0$	$\psi(z),\ \frac{1}{E-V_p}\psi(z)'$
Three band	$(E-V_s)\psi(z)+\frac{1}{3}P^2\left[\left[\frac{2}{E-V_p}+\frac{1}{E-V_0}\right]\psi(z)'\right]'=0$	$\psi(z),\ \left[\frac{2}{E-V_p}+\frac{1}{E-V_0}\right]\psi(z)'$

reduces to the earlier classical and modified Kronig-Penney models for simple structures in a simpler and more systematical way as far as the matching of boundary condition is concerned. Isolated quantum wells of an arbitrary potential profile can be calculated using the transfer matrix method as a special case of the superlattice, namely, with a very thick barrier between the bases.[5] In Secs. II and III, we describe the new Kronig-Penney models, beginning with a general theory, following by implement of envelope-function approximations, in which different potential profiles are taken into account. Finally a comparison of the three different commonly used models is made. In Secs. IV and V, the new treatise is applied to a few superlattice structures having various superlattice bases, which are important in fundamental quantum physics and device applications.

II. GENERAL THEORY

The transfer matrix technique was employed by Vassell *et al.* for calculating the transmission coefficient of resonant tunneling structures.[13] It is briefly reviewed here. Assuming that there are n layers in a tunneling structure with an active length L, the final wave function $\Gamma(z=L)$ and the initial wave function $\Gamma(z=0)$ have the relation

$$\Gamma(z=L)=S\Gamma(z=0) , \tag{1}$$

where

$$\Gamma(z)=\begin{bmatrix}\Gamma_1(z)\\ \Gamma_2(z)\end{bmatrix}$$

is a 2×1 matrix, with $\Gamma_1(z)$ representing the envelope function and $\Gamma_2(z)$ the derivative of $\Gamma_1(z)$ times a coefficient such that $\Gamma_2(z)$ is continuous throughout the active layer. $\Gamma_2(z)$ depends on the kind of models used and are listed in Table I under the column of boundary conditions. The 2×2 transfer matrix S is given by $S=S_nS_{n-1}\cdots S_1$. Each of its multiplicand S_i's is the transfer matrix of the ith single layer, and $S_i=[\Gamma^{(1)}(z=L_i),\ \Gamma^{(2)}(z=L_i)]$, where $\Gamma^{(1)}(z),\Gamma^{(2)}(z)$ are two particular solutions of Γ with initial boundary conditions $\Gamma^{(1)}(z=0)=\binom{1}{0}$ and $\Gamma^{(2)}(z=0)=\binom{0}{1}$, respectively. The thickness of the ith layer is given by L_i.

When applying to superlattices, the transfer matrix S should be for one period of the superlattice layers or the superlattice basis, and is obtained by multiplying the transfer matrices of each single layer in the basis. If d is the period of the superlattice or the length of the basis, one has

$$\Gamma(z+d)=S\Gamma(z) \quad \text{and} \quad \Gamma(z+nd)=S^n\Gamma(z) . \tag{2}$$

The eigenvalues of S are obtained by solving

$$\Gamma(z+d)=S\Gamma(z)=\lambda I\Gamma(z) . \tag{3}$$

As $n\rightarrow\pm\infty$, the limit of S^n should exist, and this implies $|\lambda|=1$ for an oscillatory wave solution. Considering also translational symmetry, acceptable values of λ are $\lambda=e^{\pm iqd}$, which define the superlattice wave vector q. The above statements illustrate the well-known Bloch theory since from Eq. (3) $\Gamma_1(z+d)=e^{\pm iqd}\Gamma_i(z)$.

Expanding the 2×2 determinant $\det(S-\lambda I)=0$ from Eq. (3), the superlattice dispersion relation can be obtained. The summation of the two roots of λ is

$$S_{11}+S_{22}=e^{iqd}+e^{-iqd}=2\cos qd ,$$

and the dispersion relation becomes

$$\cos qd=\tfrac{1}{2}(S_{11}+S_{22}) . \tag{4}$$

The superlattice wave functions are the eigenfunctions in Eq. (3). The ratio of Γ_1 and Γ_2 at an arbitrary point z_0 is

$$\frac{\Gamma_1(z_0)}{\Gamma_2(z_0)}=\frac{S_{12}}{\lambda-S_{11}} . \tag{5}$$

The wave function at z_1 can be constructed from an initial point z_0 by

$$\Gamma(z=z_1)=S(z_1,z_0)\Gamma(z=z_0)$$
$$=S(z_1,z_0)\begin{bmatrix}\dfrac{S_{12}}{\lambda-S_{11}}\\ 1\end{bmatrix}\times\text{const} , \tag{6}$$

where S_{11},S_{12} are the elements of $S(d+z_0,z_0)$ and $S(z_1,z_0)$ is the transfer matrix from z_0 to z_1. Although there are two wave functions for $\lambda=e^{\pm iqd}$, their absolute values, i.e., the square root of probability densities, are equal.

In the derivations below GaAs/$Al_xGa_{1-x}As$ will be taken as an example. All the energy levels are referenced to the valence-band maximum in GaAs.

III. IMPLANTATION OF THE ENVELOPE-FUNCTION APPROXIMATIONS

A. One-band effective-mass Kronig-Penney model

For the effective-mass model, the wave equation of the conduction-band envelope function from Table I can be reduced to

$$\psi''(z)+k^2\psi(z)=0 , \tag{7}$$

where $k^2=(2m^*/\hbar^2)(E-V_s)$, and all the notations are defined in Table II. For a constant potential, V_s is a constant. If Γ is chosen to be

$$\Gamma=\begin{bmatrix}\psi\\ \dfrac{\psi'}{m^*}\end{bmatrix} , \tag{8}$$

then the transfer matrix after solving the two particular solutions $\Gamma^{(1)}(z)$ and $\Gamma^{(2)}(z)$ becomes

$$S=\begin{bmatrix}\cos kz & \dfrac{m^*}{k}\sin kz\\ -\dfrac{k}{m^*}\sin kz & \cos kz\end{bmatrix} . \tag{9}$$

TABLE II. Notations and band parameters. The 0.6:0.4 rule is used for the band offset in the conduction and the valence bands. $Al_{0.3}Ga_{0.7}As$ is used for the barrier, and $Al_{0.1}Ga_{0.9}As$ is used for the second barrier in a step-well basis.

Notations	
m_0	Free electron mass
m_0^*	The effective mass of GaAs
$m^*(z)$	The effective mass at z, $m^*=0.067(1-x)+0.15x$ for $Al_xGa_{1-x}As$
E_{G0}	Energy band gap of GaAs
$E_G(z)$	Energy band gap of $Al_xGa_{1-x}As$, $E_G=1.519-5.405\times10^{-4}T^2/T+204+1.247x$
ψ	Conduction-band envelope function
E	The electron energy when transverse wave vectors are zeros, i.e., $k_x=k_y=0$
$V_s(z)$	The conduction-band minimum at z referred to the valence-band maximum of GaAs
$V_p(z)$	The light-hole band maximum at z referred to the valence-band maximum of GaAs
$V_0(z)$	The slit-off band maximum at z referred to the valence-band maximum of GaAs
P^2	$\frac{3\hbar^2}{4}\left[\frac{1}{m_0^*}-\frac{1}{m_0}\right]E_{G0}$ for two-band model
P^2	$\frac{\hbar^2}{2}\left[\frac{1}{m_0^*}-\frac{1}{m_0}\right]\frac{E_{G0}(E_{G0}+\Delta)}{E_{G0}+2/3\Delta}$ for three-band model
Δ	The split-off band maximum to the light-hole band maximum in GaAs; $\Delta=0.35$

If $k^2\geq0$, the energy E is above the barrier V_s, and physically it is an oscillatory wave solution. While for $k^2<0$, it is an evanescent wave solution. Equation (9) is still valid if one substitutes $k=i\kappa$ and uses the equalities, $\cos i\kappa z=\cosh\kappa z$ and $\sin i\kappa z=i\sinh\kappa z$. Using Eq. (4), one may easily verify that for the superlattice with a simple basis consisting of A and B layers, with layer thicknesses L_A and L_B, respectively, the dispersion relation is

$$\cos q(L_A+L_B)=\cos k_A L_A\cos k_B L_B-\frac{1}{2}\left[\beta+\frac{1}{\beta}\right]\sin k_A L_A\sin k_B L_B\ , \tag{10}$$

where

$$\beta=\frac{k_A}{k_B}\frac{m_B^*}{m_A^*}\ ,$$

$$k_A=\left[\frac{2m_A^*}{\hbar^2}(E-V_{sA})\right]^{1/2}\ ,$$

and

$$k_B=\left[\frac{2m_B^*}{\hbar^2}(E-V_{sB})\right]^{1/2}\ .$$

For a tilted potential, as in the case of applied field, $V_s(z)=V_s-eFz$, Eq. (7) can be changed to

$$\psi''(\xi)-\xi\psi(\xi)=0\ , \tag{11}$$

with

$$\xi=-\left[\frac{2m^*eF}{\hbar^2}\right]^{1/3}\left[z+\frac{E-V_s}{eF}\right]\ ,$$

and Eq. (8) is also changed to

$$\Gamma=\begin{bmatrix}\psi(\xi)\\ -\left[\frac{2eF}{\hbar m^{*2}}\right]^{1/3}\psi(\xi)'\end{bmatrix}\ , \tag{12}$$

where m^* is the average value through the interesting layer. The transfer matrix is found to be

$$\begin{aligned}
S_{11}&=\pi[B_i'(\xi_0)A_i(\xi)-A_i'(\xi_0)B_i(\xi)]\ ,\\
S_{12}&=\pi\left[\frac{2eF}{\hbar^2m^{*2}}\right]^{-1/3}[B_i(\xi_0)A_i(\xi)-A_i(\xi_0)B_i(\xi)]\ ,\\
S_{21}&=-\pi\left[\frac{2eF}{\hbar^2m^{*2}}\right]^{1/3}[B_i'(\xi_0)A_i'(\xi)-A_i'(\xi_0)B_i'(\xi)]\ ,\\
S_{22}&=-\pi[B_i(\xi_0)A_i'(\xi)-A_i(\xi_0)B_i'(\xi)]\ ,
\end{aligned} \tag{13}$$

where $\xi_0=\xi(z=0)$ and A_i and B_i are two linearly independent Airy functions,[14] which are solutions of Eq. (11).

In reality, the potential profile within one monolayer (one layer of As atoms and one layer of Ga/Al atoms) is linear due to the discreteness in crystal growth. Thus an arbitrary potential profile in the basis can be approximated by a piece-wise linear potential. For this case, the basis is divided into several layers. Each one has either a constant or tilted potential. The smallest possible division is the length of the monolayer. The procedure follows that first the transfer matrix in each divided layer is found, then the total transfer matrix is given by multiplying all these transfer matrixes. Finally the dispersion relation is obtained by Eq. (4).

B. Two-band and three-band Kronig-Penney models

The transfer matrices for two-band and three-band models can be obtained similarly as in Sec. III A. For a constant potential profile, the wave equation has the same form as Eq. (7), and we have for the two-band (2b) and the three-band (3b) models, respectively, the following two results:

$$k_{2b}^2=\frac{3(E-V_s)(E-V_p)}{2P^2} \tag{14}$$

and

$$k_{3b}^2=\frac{3(E-V_s)}{P^2}\left[\frac{2}{E-V_p}+\frac{1}{E-V_0}\right]^{-1}. \tag{15}$$

Γ's can be chosen as

$$\Gamma_{2b}=\begin{bmatrix}\psi\\ \dfrac{\psi'}{E-V_p}\end{bmatrix} \tag{16}$$

and

$$\Gamma_{3b}=\begin{bmatrix}\psi\\ \left[\dfrac{2}{E-V_p}+\dfrac{1}{E-V_0}\right]\psi'\end{bmatrix}. \tag{17}$$

The transfer matrices are

$$S_{2b}=\begin{bmatrix}\cos kz & \dfrac{E-V_p}{k}\sin kz\\ -\dfrac{k}{E-V_p}\sin kz & \cos kz\end{bmatrix} \tag{18}$$

and

$$S_{3b}=\begin{bmatrix}\cos kz & \dfrac{\sin kz}{k\left[\dfrac{2}{E-V_p}+\dfrac{1}{E-V_0}\right]}\\ -\left[\dfrac{2}{E-V_p}+\dfrac{1}{E-V_0}\right]k\sin kz & \cos kz\end{bmatrix}. \tag{19}$$

One may again verify that the dispersion relations for the superlattice with a simple basis consisting of layers A and B are the same as Eq. (10) with the replacement of β,

$$\beta_{2b}=\frac{k_A}{k_B}\frac{E-V_{pB}}{E-V_{pA}} \tag{20}$$

$$\beta_{3b}=\frac{k_A}{k_B}\left[\frac{2}{E-V_{pA}}+\frac{1}{E-V_{0A}}\right]\Big/\left[\frac{2}{E-V_{pB}}+\frac{1}{E-V_{0B}}\right]. \tag{21}$$

It is noted that for the two-band or three-band model a simple analytic solution cannot be obtained for the tilted potential case since all the bands are coupled and the potentials in the wave equations are no longer linear.

C. Coupling of the Γ-X intervalley transfer

The above treatise is only for momenta near the Γ point. Recently, there is increasing interest in the Γ-X coupling in [001] grown resonant tunneling structures.[15–18] The conduction-band minimum near the X point in $Al_xGa_{1-x}As$ becomes lower than the Γ point minimum when $x\geq 0.45$. Intervalley transfer from the Γ minimum to the X minimum may count for the small kinks observed in the current-voltage curves in some resonant tunneling structures with Al fraction larger than 0.45. To include this effect in our model, we adopt the boundary conditions used by Liu in treating the single barrier tunneling.[19] In our notation, these boundary conditions read

$$\begin{bmatrix}\Gamma_1(z)\\ \Gamma_2 z)\end{bmatrix}_{z=0^+}=\begin{bmatrix}\Gamma_1(z)\\ \Gamma_2(z)\end{bmatrix}_{z=0^-}+\begin{bmatrix}0 & 0\\ \dfrac{2\alpha}{\hbar^2} & 0\end{bmatrix}\begin{bmatrix}X_1(z)\\ X_2(z)\end{bmatrix}_{z=0^-}$$

and

$$\begin{bmatrix} X_1(z) \\ X_2(z) \end{bmatrix}_{z=0^+} = \begin{bmatrix} X_1(z) \\ X_2(x) \end{bmatrix}_{z=0^-} + \begin{bmatrix} 0 & 0 \\ \frac{2\alpha}{\hbar^2} & 0 \end{bmatrix} \begin{bmatrix} \Gamma_1(z) \\ \Gamma_2(x) \end{bmatrix}_{z=0^-}, \quad (22)$$

where

$$X = \begin{bmatrix} X_1 \\ X_2 \end{bmatrix}$$

is a 2×1 wave-function matrix for the X minimum, analogous to Γ in Eq. (1). The coupling coefficient α having a typical value 0.1 eV Å characterizes the intervalley transfer potential as discussed in Ref. 19. If S_Γ and S_X are denoted for the uncoupled transfer matrices for the Γ and X minima, respectively, and the notations

$$S_{\Gamma X} = S_{X\Gamma} = \begin{bmatrix} 0 & 0 \\ \frac{2\alpha}{\hbar^2} & 0 \end{bmatrix}$$

are used, then the 4×1 wave function $\begin{pmatrix} \Gamma \\ X \end{pmatrix}$ after advancing one single layer L_t has the relation

$$\begin{bmatrix} \Gamma \\ X \end{bmatrix}_{z+L_1} = \begin{bmatrix} S_\Gamma & S_{\Gamma X} \\ S_{X\Gamma} & S_X \end{bmatrix} \begin{bmatrix} \Gamma \\ X \end{bmatrix}_z, \quad (23)$$

where the transfer matrix $S(z+L_t, z)$ becomes a 4×4 matrix. The allowed minibands occur at the energies where the eigenvalues of $S(z+d, z)$ have absolute values equal to one. Our calculation for AlAs/GaAs superlattices shows that for $\alpha \leq 0.1$, the miniband structures are similar to the uncoupled ones. The coupling comes into play when $\alpha \gg 0.1$ and when there is large overlap between the uncoupled Γ and X minibands. The effect of strong coupling is to diminish the original uncoupled minibands because electrons lose energy in transferring between the Γ and X minima via the overlapped minibands.

D. Comparison

The miniband energies versus well thickness are shown in Figs. 1(a)–1(c) for these three models, respectively. The barrier width is fixed to be 31 Å (or 11 monolayers). The band parameters we used are again listed in Table II. The general trend for all the three models is that the miniband energies decrease as the width of the well increases. Also the lower the miniband energies are, the smaller their bandwidths become due to higher barriers. The two-band and three-band models give the same result in predicting the minibands for the AlGaAs system while the effective-mass model predicts too high the energy when the well is wide.

In contrast, the miniband versus barrier width of a constant well width of 130 Å is shown in Fig. 2. It indicates that the miniband location is a strong function of the well width while the miniband bandwidth is a strong function of the barrier width in this case. The minibands become discrete energy levels as the barrier become very

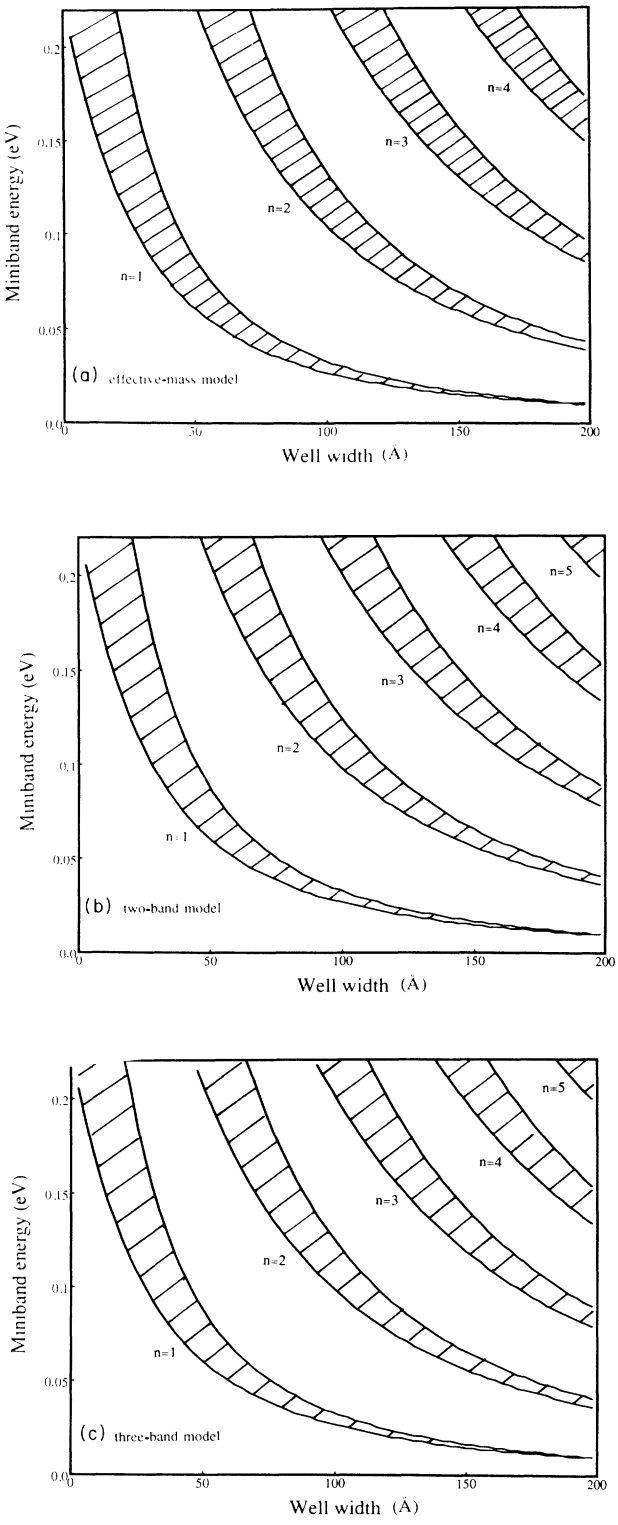

FIG. 1. The miniband energies vs well width by (a) effective-mass model, (b) two-band model, and (c) three-band model at 77 K. The barrier width is fixed to 31 Å, corresponding to 11 monolayers. Shaded areas indicate the allowed minibands. The miniband energies fall when the well width increases. The energies of the two band or three band are lower than those of the effective-mass model. The differences of the two-band and three-band models are very small.

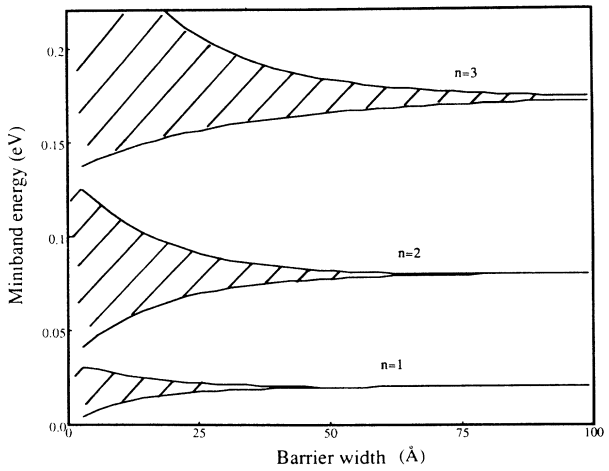

FIG. 2. The miniband energies vs barrier width by effective-mass model at 77 K. The well width is fixed to 130 Å, corresponding to 46 monolayers. The miniband width decreases when the barrier width increases while the center of the miniband is basically unchanged. As the barrier becomes very thick, the minibands of the superlattice approach discrete energy levels of isolated quantum wells.

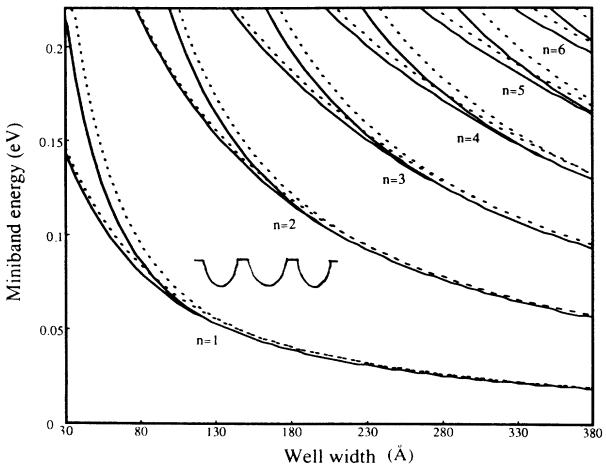

FIG. 3. Comparison of the minibands of the same parabolic well. The dotted lines indicate edges of the minibands for *n-i-p-i*, which has a constant effective mass, and the solid lines are for the compositionally gradeds well whose effective mass is changing with the barrier height. The maximum barrier height is $Al_{0.3}Ga_{0.7}As$. The barrier between each basis is 28 Å of the $Al_{0.3}Ga_{0.7}As$, corresponding to 10 monolayers.

thick in the quantum wells limit.

The advantage of the two-band or three-band model is that it includes the nonparabolicity of the bands while the limitation is that the momentum matrix element P should be a constant throughout the superlattice.[7] We have fitted P to the effective mass of GaAs but it is not accurate for AlGaAs. The accurate determination of the mini-bands location is limited by many factors, such as the error in the choice of the percentage of band offset, the inclusion of the transverse part of the energy, and the uncertainty in determining the alloy compositions and well-barrier thickness. By and large, the trend is the same and there is little difference in the result for all the three models used here. The effective-mass model is used for the following calculations.

IV. APPLICATION TO SINGLE-WELL BASIS

A. Parabolic quantum well

Although the parabolic well is usually the building block of the doping superlattices or *n-i-p-i*,[20] the growth of it by grading the alloy composition is also possible.[11,21,22] Theoretical calculations for a parabolic well under an applied electric field were done analytically[23] or numerically[24] just recently. Using our method, the minibands of a superlattice made of parabolic basis are shown in Fig. 3. Also shown are the minibands of the *n-i-p-i* structure which has a constant effective mass otherwise the same potential in the conduction band. Our new model is especially useful when the carrier injection needs to be considered as in *n-i-p-i* structures for current controlled band tunning applications.[20]

B. Triangular well

The miniband energies in a rectangular-well superlattice can be simply estimated as $E_n \propto n^2$, where n denotes the nth miniband. For the applications of band-aligned superlattices(BAS),[10] sometimes it is necessary to use a different kind of superlattices in order to provide a miniband discontinuity. This dissimilar superlattice has the miniband energy $E_n \propto n^a$, where $a < 2$. The parabolic well in the previous case has $a \approx 1$. Another example is the triangular well with $a < 1$ as shown in Fig. 4. The bandwidth of the triangular well superlattice decays faster than the parabolic well or the rectangular well since the barrier increases very fast. Also the ground-state band has higher energy than the other wells due to the narrowing toward the bottom of the well.

It should be noted that the channel of the high-electron-mobility transistor (HEMT) is often approximated as a triangular potential well. The exact calculation of the energy levels is possible in our treatise to include doping and the carrier accumulation effects on the potential shape.

C. Step-well superlattice

The step-well shown in the inset of Fig. 5 also falls into the superlattice group with $a < 2$. With the change of the alloy composition and the width of the well, the step well is more flexible than the parabolic well or triangular well in the BAS application. Our recent calculation also shows that the step quantum well has large intersubband Stark shift in that the energy levels in the small and big wells have different dependence on the electric field. A

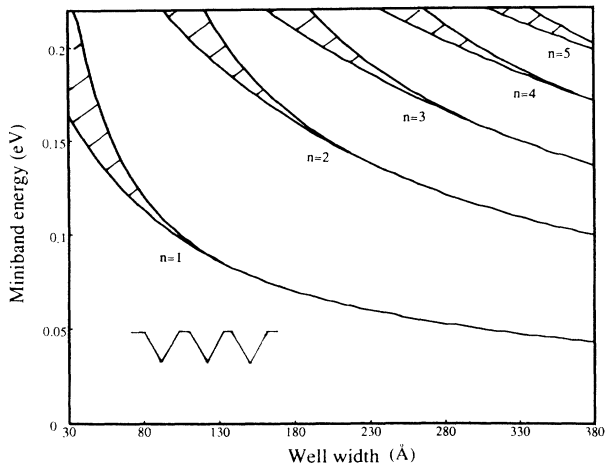

FIG. 4. The minibands of a triangular-well superlattice. The structure of a triangular-well superlattice is shown in the inset. The maximum barrier height is $Al_{0.3}Ga_{0.7}As$. The barrier between each basis is 28 Å of the $Al_{0.3}Ga_{0.7}As$, corresponding to 10 monolayers. The gaps between minibands are decreasing toward the top of the barrier.

plot of E-k dispersion relation is shown in Fig. 5 for the rectangular well, parabolic well, triangular well, and step well, respectively, where the lower bands are deliberately chosen to be aligned, thus a miniband discontinuity is formed for the upper band. The triangular well and step well have the most desired features.

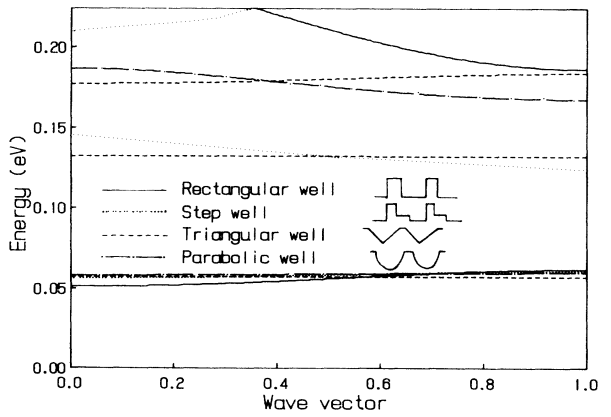

FIG. 5. Comparison of the E-k dispersion relation for the rectangular well, parabolic well, triangular well, and the step well. The structures are shown in the inset. The barrier and well widths used in the calculation are 40 Å, 62 Å, for the rectangular well; 40 Å, 74 Å (the second barrier), 34 Å for the step well; 14 Å, 246 Å for the triangular well; and 28 Å, 116 Å for the parabolic well, respectively. We assume $Al_{0.3}Ga_{0.7}As$ for the barrier and $Al_{0.1}Ga_{0.9}As$ for the second barrier of the step well. The lower minibands are deliberately chosen to be aligned. The upper minibands of the triangular well and the step well are the lowest.

V. APPLICATION TO MULTIPLE-LAYER BASIS

A. Two-well coupling

The coupling of two quantum wells is found to have more energy levels than the single quantum well of the same dimensions.[25] Large Stark shift has been found in coupled quantum wells.[9,26,27] Our theoretical calculation of the minibands is shown in Fig. 6 for a superlattice basis consisting of two rectangular wells, one of the well widths is fixed (90 Å) and the other varied. Compared to Fig. 1(a), it is clear that in the two-well case the minibands are mixed from those of its original wells. The two horizontal bands in Fig. 6 indicate the energy levels for the 90 Å well. While the four falling bands are the minibands of the variable well. The miniband bandwidth is narrow in this case because the other well acts as a barrier when one looks from one well.

B. Band-aligned basis

The cross points in Fig. 6 are where the minibands of the two wells are aligned. The first cross point occurs when the varied well width is 25 Å, where its only miniband is aligned with the upper miniband of the 90 Å well. The aligned bands have much larger bandwidth than the nonaligned bands which are bound states in natural, since the nonsymmetrical well acts as a barrier for the nonaligned minibands.

One application of the band-aligned basis is to use the bound state to miniband transition which has a significant effect in improving the dark current for the photo detectors.[12] The major advancement in using intersubband transition for 8–12 μm detection is the reduction of dark current.[28,29] If thicker barriers are used, the

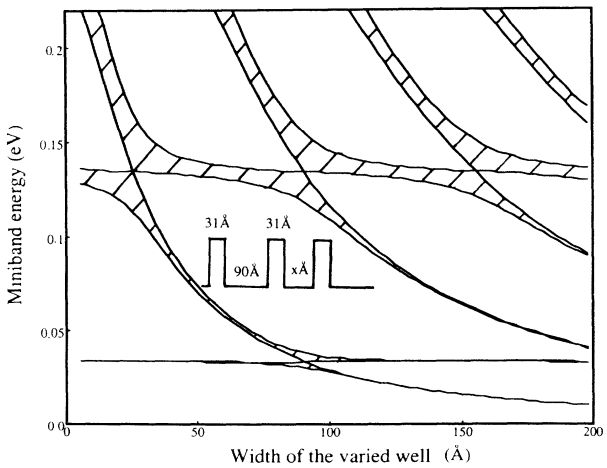

FIG. 6. The minibands of a superlattice with the basis consisting of two coupled wells. One of the well is fixed to be 90 Å, and the other is changed as a parameter. The two barriers in the basis are fixed to be 31 Å. It superimposes the minibands originated from each well. As the bands cross over, band alignment occurs, but are soon split off.

photocurrent will decrease due to the same reason of a low dark current. The employment of band-aligned basis will reduce the dark current because of the bound-state nature of the lower nonaligned band while the conductivity is large in the upper aligned band.

Another application of the band-aligned basis is the tunning of the mobility or the effective-mass ratio of the upper to the lower miniband. The effective mass m_z of the miniband is related to the miniband bandwidth B by $m_z = 2\hbar^2/Bd^2$, where d is the length of the basis. This relation is easily obtained by taking the second derivative of the miniband dispersion relation $E = E_0 + \frac{1}{2}B\cos qd$. Thus for a band-aligned basis, the effective-mass ratio of an aligned band to the bound state is significantly different from the conventional structures. For the rectangular-well superlattice the bandwidth ratio for the second band to the ground band is on the orders of 5–10, but for the case of band-aligned basis, it can be more than 10^3. To reduce this bandwidth ratio, one may choose to align to the lower band instead of the upper band. An example is shown in Figs. 7(a) and 7(b) for the band alignment in the upper and the lower bands, respectively. The bandwidth ratio is about unity in the latter.

C. Perturbation of degenerate states in quantum wells

The crosspoints in Fig. 6 reveal that the bands only align in one point; beyond that point of the well width the aligned bands will split into two. The same energy tends to repel one from the other.

For further investigations, the two coupled well basis is again used as an example. This time the two wells are identical, with one variable barrier width. As shown in Fig. 8 the original states of either of the wells have two minibands, the lower one is 31–39 meV and the upper one is 119–151 meV. The variable barrier perturbs the degenerate states and each of the minibands will split into two.

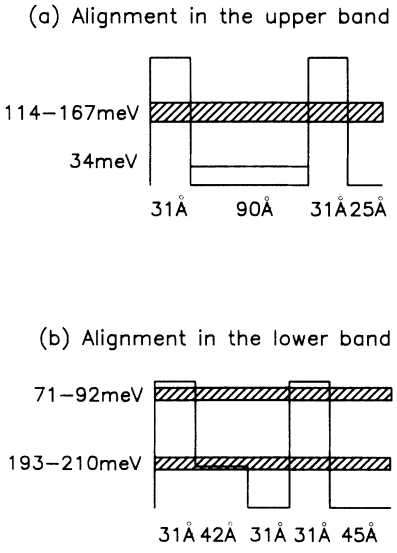

FIG. 7. Structures of band-aligned bases; alignment can be done either (a) in the upper band or (b) in the lower band. In (a), the widths of the two coupled wells are 90 Å, 25 Å, respectively. The barrier width is 31 Å. In (b), the basis consisting of a step well and a rectangular well. The alloy compositions and the layer widths are 0.3, 0.1, 0, 0.3, and 0 and 31 Å, 42 Å, 31 Å, 31 Å, and 45 Å, respectively. The bandwidth in the lower band is about equal to that in the upper band.

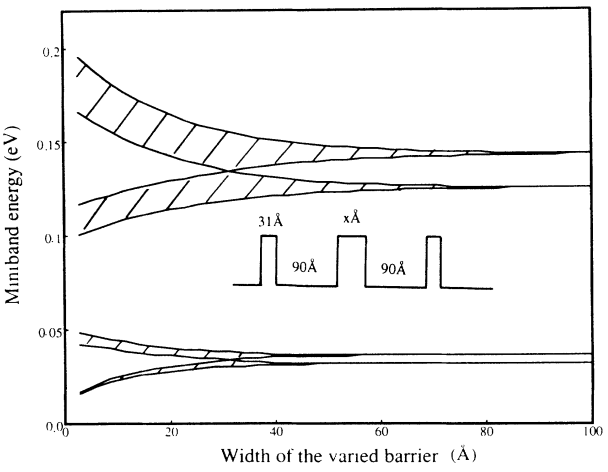

FIG. 8. The demonstration of perturbation of two degenerate minibands in the superlattice. The basis consists of two identical wells with width 90 Å, one fixed barrier with a 31 Å width and the other barrier with varied width as a parameter. The original miniband has split into two because of the perturbation.

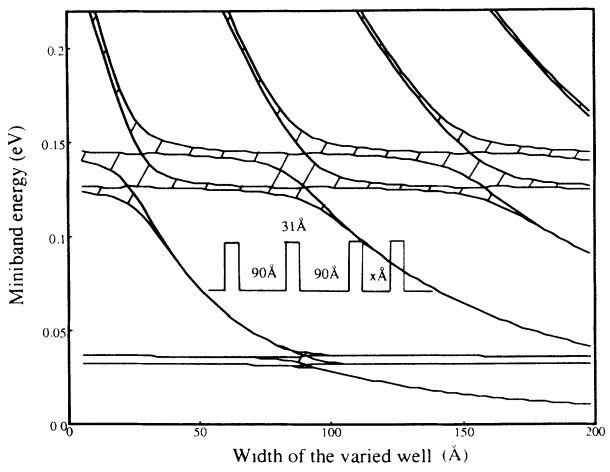

FIG. 9. The miniband structures of a basis with three coupled wells. Two of the wells are identical and fixed, with the other changed. The fixed wells have a width of 90 Å. All the barriers are fixed to be 31 Å. The band structures result from superpositions of all the minibands originated from the single well basis, with the repulsion effect taken into consideration.

D. Multiple well coupling

Physically, the miniband structures of a multiple layer basis can be treated as a mixture or superposition of the states originated from the single-well basis, with the perturbation taken into account if the energy levels are too close to each other. The wave functions are oscillatory in its own original well and decaying in all the other wells and barriers. In the case of three-well coupling, we choose two identical wells and one varied well as shown in Fig. 9. Each of the original minibands of the identical wells split into two bands because the varied well is a perturbation for the degenerate minibands, otherwise all the bands retain their original shapes.

VI. CONCLUSION

In the first part of the paper, a new formalism of the Kronig-Penney model has been developed which incorporates the transfer matrix technique and the envelope-function approximations. This new approach has several advantages over the other methods. First, its formalism by transfer matrix is much easier and more systematic than the conventional Kronig-Penney model as far as the boundary condition matching is concerned. Second, it can calculate for complicated multiple layer bases and arbitrary potential profiles result from change of alloy composition, doping or carrier accumulation. Third, it is accurate and without excessive computation cost since the effective-mass difference, nonparabolicity and band coupling of the bulk bands are included by the envelope function in a natural way.

In the second part of the paper, our new approach is applied to some specific superlattice bases. The finite parabolic well case is solved in a simpler and more accurate way. The triangular well and step well which belong to the superlattices with $E_n \propto n^a, a < 2$, which are useful in the BAS applications can also be easily worked out. The minibands of a superlattice with the basis consisting of multiple layers can be considered as a superposition of all the minibands originated from their simple single-well basis, with the repulsion effect taken into account. The method offered to us explains readily the coupling of wells in the basis for tunning the energy levels. The splitting of minibands, the band-aligned basis, the overlapping of the wave functions originated from different wells, and the effective-mass tunning in superlattices are among the examples.

ACKNOWLEDGMENT

The authors are indebted to Dr. J. Schulman in the discussion of the envelope-function approximations. The discussions with Dr. R. Karunasiri and Mr. Y. Mii are also helpful. This work is supported in part by Office of Naval Research, Army Research Office, and Semiconductor Research Corporation.

[1]Leo Esaki, IEEE J. Quantum Electron. **QE-22**, 1611 (1986).
[2]L. Esaki and R. Tsu, IBM J. Res. Dev., Jan. 1970, p. 61.
[3]G. Bastard, Phys. Rev. B **24**, 5693 (1981).
[4]G. Bastard and J. A. Brum, IEEE J. Quantum Electron. **QE-22**, 1625 (1986).
[5]G. Bastard, in *Molecular Beam Epitaxy and Heterostructures*, Vol. 87 of *NATO Advanced Study Institute Series E*, edited by L. L. Chang and K. Ploog (Martinus Nijhoff, Dordrecht, 1985), pp. 381–423.
[6]E. O. Kane, J. Phys. Chem. Solids **1**, 249 (1957).
[7]Joel N. Schulman, Mater. Res. Soc. Symp. Proc. **56**, 279 (1986).
[8]Hung-Sik Cho and Paul R. Prucnal, Phys. Rev. B **36**, 3237 (1987).
[9]H. Q. Le, J. J. Zayhowski, and W. D. Goodhue, Appl. Phys. Lett. **50**, 1518 (1987).
[10]Perng-fei Yuh and K. L. Wang, Appl. Phys. Lett. **51**, 1404 (1987).
[11]Susanta Sen, Federico Capasso, Arthur C. Gossard, Richard A. Spah, Albert L. Hutchinson, and S. N. G. Chu, Appl. Phys. Lett. **51**, 1428 (1987).
[12]K. K. Choi, B. F. Levine, C. G. Bethea, J. Walker, and R. J. Malik, Phys. Rev. Lett. **59**, 2459 (1987).
[13]M. O. Vassell, Johnson Lee, and H. F. Lockwood, J. Appl. Phys. **54**, 5206 (1983).
[14]*Handbook of Mathematical Functions*, edited by M. Abramowitz and I. A. Stegun (National Bureau of Standards, Washington, D. C., 1964).
[15]I. Hase, H. Kawai, K. Kaneko, and N. Watanabe, J. Appl. Phys. **59**, 3792 (1986).
[16]E. E. Mendez, W. I. Wang, E. Calleja, and C. E. T. Goncalves da Silva, Appl. Phys. Lett. **50**, 1263 (1987).
[17]A. C. Marsh, IEEE J. Quantum Electron. **QE-23**, 371 (1987).
[18]A. R. Bonnefoi and T. C. McGill, Phys. Rev. B **37**, 8754 (1988).
[19]H. C. Liu, Appl. Phys. Lett. **51**, 1019 (1987).
[20]Gottfried H. Döhler, IEEE J. Quantum Electron. **QE-22**, 1682 (1986).
[21]R. C. Miller, A. C. Gossard, D. A. Kleinman, and O. Munteanu, Phys. Rev. B **29**, 3740 (1984).
[22]S. Y. Chou and J. S. Harris, Jr., Appl. Phys. Lett. **52**, 1422 (1988).
[23]R. P. Karunasiri and K. L. Wang, Superlatt. Microstruct. (to be published).
[24]Yang Chu-liang and Yang Qing, Phys. Rev. B **37**, 1364 (1988).
[25]Herbert Kroemer and Hiroshi Okamoto, Jpn. J. Appl. Phys. **23**, 970 (1984).
[26]Y. J. Chen, Emil S. Koteles, B. Elman, and C. A. Armiento, Mater. Res. Soc. Symp. Proc. **102**, 571 (1988).
[27]Perng-fei Yuh and K. L. Wang, Phys. Rev. B **38**, 8377 (1988).
[28]B. F. Levine, K. K. Choi, C. G. Bethea, J. Walker, and R. J. Malik, Appl. Phys. Lett. **50**, 1092 (1987).
[29]K. K. Choi, B. F. Levine, C. G. Bethea, J. Walker, and R. J. Malik, Appl. Phys. Lett. **50**, 1814 (1987).